Smith, G. N., Finlayson, S. D., Gillespie, D. A. J., Peach, J., Pegg, J. C., Rogers, S. E., Shebanova, O., Terry, A. E., Armes, S. P., Bartlett, P., & Eastoe, J. (2016). The internal structure of poly(methyl methacrylate) latexes in nonpolar solvents. *Journal of Colloid and Interface Science*, *479*, 234-243. https://doi.org/10.1016/j.jcis.2016.06.027

# The internal structure of poly(methyl methacrylate) latexes in nonpolar solvents

Gregory N. Smith[a,b,*], Samuel D. Finlayson[a], David A. J. Gillespie[a,1], Jocelyn Peach[a], Jonathan C. Pegg[a], Sarah E. Rogers[c], Olga Shebanova[d], Ann E. Terry[c], Steven P. Armes[b], Paul Bartlett[a], Julian Eastoe[a]

[a] *School of Chemistry, University of Bristol, Cantock's Close, Bristol, BS8 1TS, UK*
[b] *Department of Chemistry, University of Sheffield, Dainton Building, Brook Hill, Sheffield, South Yorkshire, S3 7HF, UK*
[c] *ISIS-STFC, Rutherford Appleton Laboratory, Chilton, Oxon OX11 0QX, UK*
[d] *Diamond Light Source Ltd, Diamond House, Harwell Science and Innovation Campus, Chilton, Didcot, OX11 0DE, UK*

**Abstract**

*Hypothesis.* Poly(methyl methacrylate) (PMMA) latexes in nonpolar solvents are an excellent model system to understand phenomena in low dielectric media, and understanding their internal structure is critical to characterizing their performance in both fundamental studies of colloidal interactions and in potential industrial applications. Both the PMMA cores and the poly(12-hydroxystearic acid) (PHSA) shells of the latexes are known to be penetrable by solvent and small molecules, but the relevance of this for the properties of these particles is unknown.

*Experiments.* These particles can be prepared in a broad range of sizes, and two PMMA latexes dispersed in *n*-dodecane (76 and 685 nm in diameter) were studied using techniques appropriate to their size. Small-angle scattering (using both neutrons and X-rays) was used to study the small latexes, and analytical centrifugation was used to study the large latexes. These studies enabled the calculation of the core densities and the amount of solvent in the stabilizer shells for both latexes. Both have consequences on interpreting measurements using these latexes.

*Findings.* The PHSA shells are highly solvated ($\sim$ 85 % solvent by volume), as expected for effective steric stabilizers. However, the PHSA chains do contribute to the intensity of neutron scattering measurements on concentrated dispersions and cannot be ignored. The PMMA cores have a slightly lower density than PMMA homopolymer, which shows that only a small free volume is required to allow small molecules to penetrate into the cores. Interestingly, the observations are essentially the same, regardless of the size of the particle; these are general features of these polymer latexes. Despite the latexes being used as a model physical system, the internal chemical structure is complex and must be fully considered when characterizing them.

*Keywords:* Nonpolar solvents; Latexes; Small-angle scattering; Analytical centrifugation

**Graphical abstract**

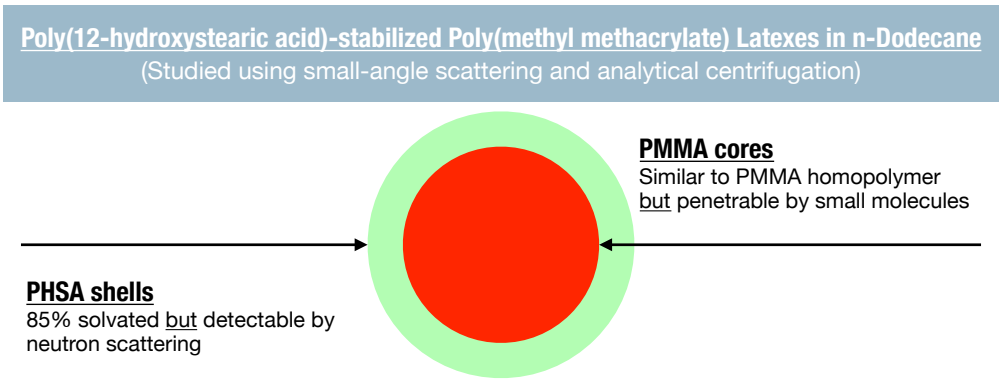


## 1. Introduction

Dispersions of colloids in nonpolar solvents are prevalent in soft matter nanoscience [1–12]. The significance of such dispersions can be appreciated by considering the many various industrial sectors that make use of them, which include petrochemicals [13], lubricants [7, 14, 15], reprography [4, 5], inkjet printing [5], magnetic recording media [4], rheological fluids [16, 17], and electronic displays [18–21]. Poly(methyl methacrylate) (PMMA) latexes, originally developed through an industrial-academic collaboration between the University of Bristol and ICI [22, 23], have proved an essential tool for colloid scientists to develop new technologies and study fundamental interactions in nonpolar media. These PMMA latexes are typically sterically-stabilized with poly(12-hydroxystearic acid) (PHSA) brushes, although there is active research into developing other effective steric stabilizers [8, 24–28]. They are generally dispersed in either *n*-alkanes or in mixed solvents to achieve density or refractive index matching (typically decalin and either brominated cycloalkanes or carbon disulfide) [29–34]. The latexes are a particularly useful model system because it is possible to reproducibly synthesize particles of a desired size with a narrow size distribution [23, 35–39]. This has enabled many enlightening studies into phenomena such as hard-sphere colloidal crystallization [29–33, 40, 41], ionic crystallization [34, 42, 43], depletion-induced gelation and glass formation [44, 45], and the interaction of charges in low dielectric media [10, 46–50].

Despite these PMMA latexes being an excellent *physical* model system, it is underappreciated that their *chemical* composition is far from simple [38]. By failing to account for their internal structure, important interactions of components, present even at small concentrations, at the surface or interior of the latexes may be overlooked. The PHSA stabilizer that is used to stabilize latexes during synthesis is a brush polymer consisting of typically pentamer or hexamer HSA polyesters with a backbone of MMA and glycidyl

*Corresponding author
*Email address:* g.n.smith@sheffield.ac.uk (Gregory N. Smith)
[1]Current address: Croda Europe, Cowick Hall, Snaith, Goole, East Yorkshire, DN14 9AA, UK

methacrylate (GMA) to enable chemical grafting to the surface of the latexes. The cores consist of predominantly PMMA but also include a thiol chain transfer agent and methacrylic acid monomer (MAA), which reacts with the GMA. Grafting is promoted by adding, typically, diethanolamine [51] to catalyze the GMA-MAA esterification reaction. The effect of the chemical constituents can be seen by considering either the shell or core of the latexes. For example, differences in the precursor materials can have an effect on their properties: varying the purity of the HSA monomer or the specific details of the synthesis can change the degree of polymerization of the PHSA brushes [38, 52] and using different amine catalysts can change the polarity of charged latexes [53]. Additionally, the solvent can influence the properties of the latexes. This study focusses on particles dispersed only in an $n$-alkane. The use of cosolvents to achieve refractive index or density matching are known to interact with the particles, though either swelling the latexes or inducing charge [54, 55]. The use of cosolvents that are good solvents for PMMA is also known to swell particles [56, 57]. While this study focusses only on $n$-dodecane, the approach used here could be extended to other solvents to characterize latexes used for different purposes.

Depending on the physical model being investigated or the potential application being targeted, particles of very different sizes may be desirable. By varying the relative concentrations of the PHSA stabilizer and the core-forming PMMA, particles can be synthesized with a range of sizes: from less than 60 nm [51] to greater than 2.5 $\mu$m [23]. This spans lengthscales that are relevant for many studies, including small-angle scattering of small particles [51, 58] or confocal microscopy studies on large particles [31–33], for example. Clearly, the fraction of stabilizer and core varies significantly between these limits. It is not possible to predict the effect that changing the relative fractions of stabilizer and core polymers would have on the internal structure of the latexes. In order to study this, two latexes (with solvodynamic diameters of 76 nm and 685 nm) have been prepared to examine the internal structure of latexes of different sizes. Thus, it should be possible to determine whether or not the internal structure is size-dependent. Two methods appropriate to the size of the latexes were used to study the composition of the latexes in $n$-dodecane: small-angle scattering and analytical centrifugation. Small-angle scattering has been extensively used before to study these latexes, but this is a rare example of the use of analytical centrifugation. By using these complementary techniques, the properties of the latexes are found to be independent of the particle size.

Studies on these PMMA latexes in the literature have typically used different batches of precursor chemicals. In this study, by using the same batches of stabilizer and monomers, particles have designed to, as much as possible, differ only in their diameter, enabling any differences to be ascribed to the size of the particles. The properties of interest are the volume fraction of solvent in the steric stabilizer shells (relating to solvation due to the extension of the brushes into the solvent) and the density of the polymer cores (relating to the similarity between the latex cores and PMMA homopolymer). The precise characterization enabled by modern scattering and centrifugation equipment means that detail about these model colloids has been revealed with high resolution. Quantifying the properties of latexes of different sizes will enable

aspects of their chemical complexity to be better understood. These results do not simply present significant understanding of the internal structure of PMMA latexes in nonpolar solvents, but they should also inform future experiments making use of these model colloids. Given the many uses of colloids in nonpolar solvents in applied and fundamental research, the use of different nonpolar solvents to obtain desirable properties, and the desire to generate new stabilizers for hydrocarbon solvents, these results should aid the development of research into dispersions in low dielectric media.

## 2. Experimental

### *2.1. Latex synthesis*

Two dispersions of PMMA latexes (GS1 and SF1) were prepared by nonaqueous dispersion polymerization using the method described by Antl *et al.* [23]. The formulations used to prepare these particles is shown in Table 1.

Table 1: Formulations for GS1 and SF1 PMMA latexes (masses in g)

| Latex | MMA | MAA | Stabilizer[a] | AIBN | *n*-Hexane | *n*-Dodecane | 1-Octanethiol |
|---|---|---|---|---|---|---|---|
| GS1 | 6.312 | 0.155 | 4.690 | 0.080 | 7.699 | 0.435 | 0.028 |
| SF1 | 10.0158 | 0.1943 | 1.8565 | 0.1015 | 7.0511 | 4.1374 | 0.0589 |

[a] Mass given is for 27 wt. % solution of PMMA-*graft*-PHSA in *n*-dodecane.

The monomer mixture (predominantly methyl methacrylate (MMA) with a small amount of methacrylic acid (MAA)), PMMA-*graft*-PHSA brush copolymer stabilizer, azobisisobutyronitrile (AIBN) initiator, 1-octanethiol chain transfer agent, and the solvent mixture (*n*-hexane and *n*-dodecane) were weighed into a three-neck round bottom flask. A condenser and septum were attached to the round bottom flask, and a magnetic stirrer bar was used to stir the reaction. The reaction mixture was purged with nitrogen gas before being placed in a oil bath preheated to 80°C. The reaction was monitored to ensure that nucleation occurred (when it turned opalescent) and was conducted for 2 h, in accordance with literature [23, 35, 36]. Diethanolamine in *n*-dodecane (mass equal to *n*-hexane) was then added to fix the stabilizer to the particle surface. The temperature was increased to 120°C, and the surface locking reaction was run for 18 h. The crude dispersion was filtered through glass wool to remove any aggregates.

The particles were purified by centrifugation. The GS1 dispersion was centrifuged at 10,000 rpm for 3 h, and the SF1 dispersion was centrifuged at 6,000 rpm for 1 h. Each time, the supernatant liquid was removed. Fresh *n*-dodecane was added, and the particles were redispersed. This was repeated five times.

### *2.2. Methods*

#### *2.2.1. Dynamic light scattering) DLS*

Dynamic light scattering measurements were performed using a Malvern Zetasizer Nano S90 on dilute dispersions in *n*-dodecane. Data were processed in the Malvern Zetasizer Software. *Z*-average diameters and

polydispersity indexes (PdIs) were determined using cumulants analysis along with intensity-weighted distributions, which were calculated and then converted to volume-weighted and number-weighted distributions using Mie theory.

*2.2.2. Small-angle X-ray scattering (SAXS)*

X-ray scattering measurements were performed using the instrument I22 at Diamond Light Source. Samples were measured in 1 mm capillaries, and data were recorded on a PILATUS 2M detector. The sample-detector distance was 9.4 m, and two X-ray wavelengths were used ($\lambda$ = 1.77 Å, $E$ = 7 keV, $Q$ = 0.001–0.11 Å$^{-1}$ and $\lambda$ = 0.73 Å, $E$ = 17 keV, $Q$ = 0.003–0.27 Å$^{-1}$). Raw scattering data were radially integrated using YAX 2.0, a macro script for ImageJ [59, 60], normalized for measurement time, and the empty cell and solvent background subtracted to give scattering cross-sections. Data were fit to models as described in the text using the SasView small-angle scattering software package [61] and weighted by $|\sqrt{I(Q)}|$.

*2.2.3. Small-angle neutron scattering (SANS)*

Neutron scattering measurements were performed at the ISIS Pulsed Neutron Source. On Sans2d, a simultaneous $Q$-range of 0.003–0.43 Å$^{-1}$ was achieved using an instrument set up with the source-sample and sample-detector distances of $L_1$=$L_2$=8 m and the 1 m$^2$ detector offset vertically 60 mm and sideways −290 mm [62]. On LOQ, data were recorded on a single two-dimensional detector to provide a simultaneous $Q$-range of 0.008–0.24 Å$^{-1}$ using neutrons with $2 \leq \lambda \leq 10$ Å [63]. The beam diameter was 8 mm. Raw scattering data sets were corrected for the detector efficiency, sample transmission, and background scattering and radially averaged using the instrument-specific software, Mantid. These data were placed on an absolute scale (cm$^{-1}$) using the scattering from a standard sample (a solid blend of hydrogenous and perdeuterated polystyrene) [64]. Data have been fit to models as described in the text using the SasView small-angle scattering software package [61].

*2.2.4. Analytical centrifugation*

Analytical centrifugation was performed using a LUMiSizer analytical photocentrifuge (LUM GmbH, Berlin, Germany). The temperature was 25°C, and measurements were performed on latex dispersions at a concentration of 1 wt. % in *n*-dodecane and at a volume fraction equivalent concentration in *n*-dodecane-$d_{26}$ (0.79 wt. %). For the dispersion in *n*-dodecane-$d_{26}$, a concentrated dispersion was transferred into the isotopically-labeled solvent by centrifugation and redispersal in fresh solvent (centrifugation at 6,000 rpm for 1 h, repeated three times) and then diluted using *n*-dodecane-$d_{26}$. The latexes were centrifuged at 1,000 rpm in 2 mm path-length polyamide cells. The sedimentation process was monitored as a function of time across the entire cell using STEP Technology (space- and time-resolved extinction profiles), enabling determination of the sedimentation velocities or the particle size distributions.

## 3. Results

### *3.1. Latex size*

The mean size and the distribution of the latexes were determined first to enable realistic parameters to be inputted into subsequent analysis. Dynamic light scattering was used to characterize the latexes initially. This technique measures the intensity-weighted solvodynamic diameter of the latexes; therefore, the size of the core as well as the thickness of the shell contributes to the size determined.

Size distributions of the two latexes are shown in Figure 1. The $Z$-average diameters ($d_Z$) determined from cumulants analysis are 76 nm (PdI = 0.10) for the GS1 latexes and 685 nm (PdI = 0.17) for the SF1 latexes. The size distributions shown in Figure 1 can be used to determine the intensity-weighted diameters ($d_i$) from the location of the peak. They were found to be similar to the $Z$-average diameters. The values of $d_i$ are 84 nm for the GS1 latexes with a polydispersity ($\sigma$, standard deviation divided by mean) of $\sigma = 0.31$ and 683 nm for the SF1 latexes with $\sigma = 0.19$.

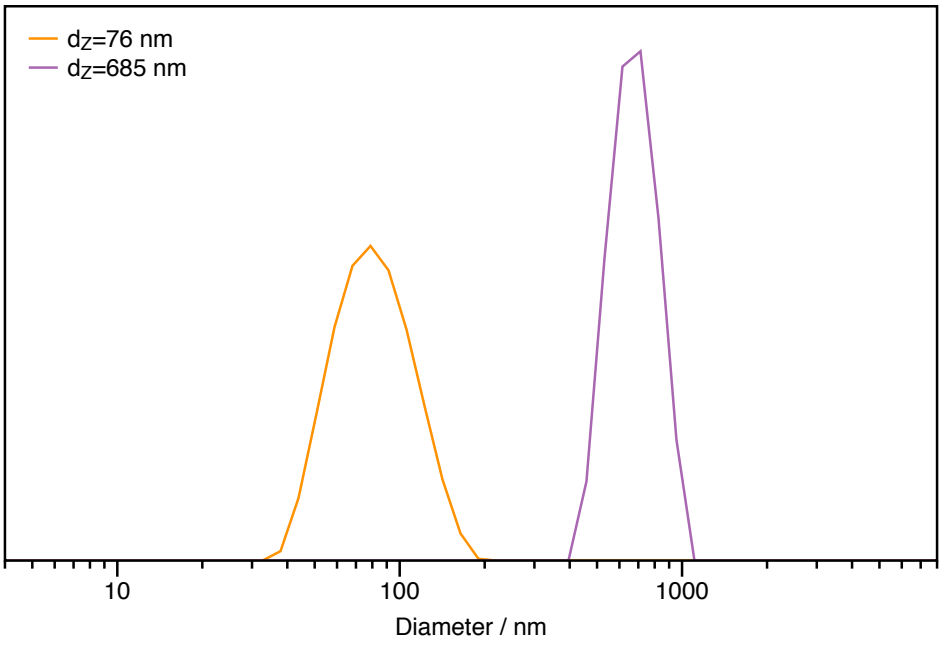


Figure 1: Diameters of the PMMA latexes used in this study measured using DLS. The $Z$-average diameters are given in the legend. The peaks of the intensity-weighted size distributions giving diameters that correspond to the $Z$-average diameters.

In addition to DLS, which is sensitive to the whole diameter of the latex, techniques that are sensitive to the cores and appropriate to the size of the two latexes were used. Small-angle X-ray scattering (SAXS) was used to study the 76 nm diameter latexes (the stabilizer shells have no X-ray contrast with the solvent), and scanning electron microscopy (SEM) was used to study the 685 nm diameter latexes (the stabilizer shells collapse under vacuum).

Core size distributions of the two latexes are shown in Figure 2. The SAXS curve of the smaller 76 nm diameter latexes was fit to a spherical form factor [65, 66] with a log-normal size distribution [51, 58]. The PHSA stabilizer has the same electron density as the $n$-dodecane solvent and, therefore, no X-ray contrast. Because of this, SAXS data on the latexes can be fit assuming a simple sphere form factor. The diameter of the cores was found to be 57 nm with a distribution width of $\sigma = 0.09$, and the resulting size distribution is plotted in Figure 2. (The raw SAXS curve is shown in the Electronic Supplementary Material.) The SEM histogram (418 particles) of the larger 685 nm latexes was processed with 10 nm bins, and the curve fit to a log-normal distribution. The diameter of the cores was found to be 660. nm with a size distribution width of $\sigma = 0.05$. (A typical SEM image is shown in the Electronic Supplementary Material.) These core sizes are consistent with the $Z$-average solvodynamic radii of the particles measured using DLS. The DLS radii are greater than those determined by SAXS or SEM because the solvodynamic radius includes the size of the stabilizer shells. Additionally, the weighting of the diameters determined by the techniques are different: DLS reports intensity-weighted diameters whereas SAXS reports volume-weighted diameters and SEM reports number-weighted diameters. Therefore, the peaks in these differently weighted distributions also need to be compared. The raw DLS intensity-weighted distributions were converted to the appropriate weighting and are shown in Figure 2. The distributions from the different techniques compare well. The difference in the radii of the 76 nm latexes measured using SAXS and DLS can be accounted for by the thickness of the stabilizer layer, which will be discussed later. The fact that the DLS $d_n$ is smaller than the SEM $d_n$ is contrary to this assertion. However, due to processing required to determine the number-weighted DLS distribution and how broad it is, this difference can be accounted for by experimental uncertainty.

### *3.2. 76 nm diameter latexes*

Small-angle scattering (SAS) has been used in the literature to study small latexes (typically $< 100$ nm). Small-angle neutron scattering (SANS) has been used to study the composition and interaction of latexes by the Ottewill group at the University of Bristol [51, 58, 67–70] and others [71, 72] as well as to study the distribution of surfactants in charged latexes [73–76]. Small-angle X-ray scattering (SAXS) has also been used to study the interaction of such PMMA latexes [77, 78]. Recently, spin-echo SANS (SESANS) has also been used to study the composition and interactions of latexes [79]. Modern SAS instrumentation enables more detailed analysis of nanoparticles over a broader $Q$-range, and consequently size range, with increased intensity resolution than was possible in the past.

The internal structure of the small 76 nm (GS1) latexes was studied using both SANS and SAXS. SAXS characterization of a dilute dispersion of 76 nm latexes was discussed in Section 3.1. Contrast variation-SANS (CV-SANS) was further used to characterize the latexes by determining the scattering length density (SLD, $\rho_{\mathrm{n}}$). CV-SANS is an approach where the SLD of the solvent is varied to modify the intensity of scattering arising from certain species. The scattering intensity per unit volume ($I(Q)$) is defined as the product of the

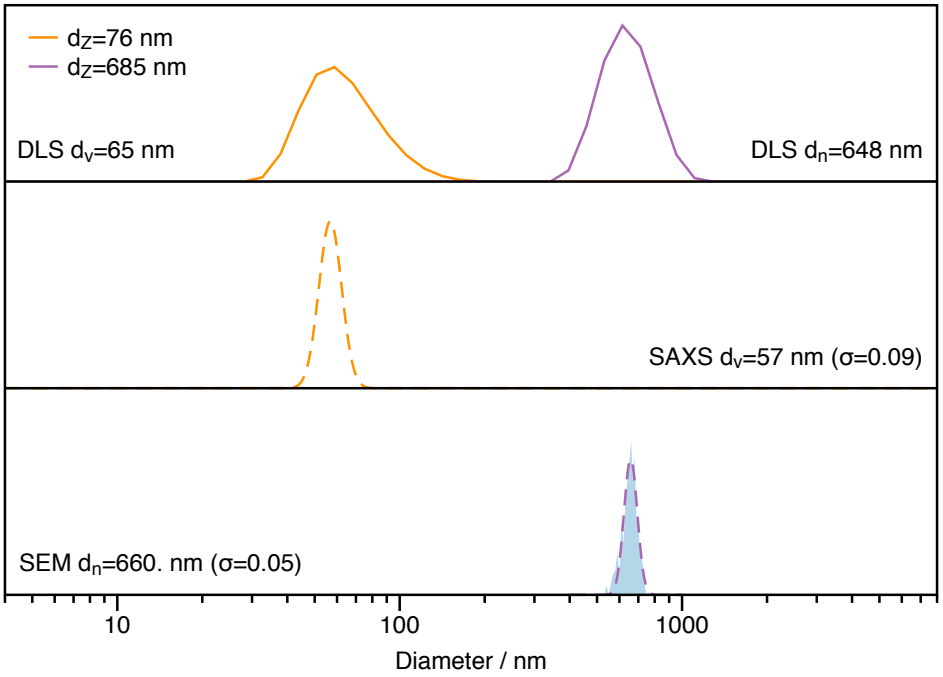


Figure 2: Diameters of the cores of PMMA latexes compared to DLS diameters. The core diameters are measured using techniques sensitive only to the polymer cores and appropriate to the particle sizes: small-angle X-ray scattering (SAXS) for the 76 nm latexes and scanning electron microscopy (SEM) for the 685 nm latexes. The dimensions determined are shown in the labels. The appropriately weighted DLS distributions are shown depending on the technique used to size the cores: volume-weighted for SAXS and number-weighted for SEM.

volume fraction ($\phi$), the volume of the particles ($V_p$), the difference in SLD between solvent and scattering particles ($\Delta\rho_{\mathrm{n}}$), the form factor ($P(Q)$), and the structure factor ($S(Q)$). $P(Q)$ is determined from the particle morphology, and $S(Q)$ is determined from the particle interactions, which are only significant for concentrated dispersions [80].

$$I(Q) = \phi V_p \Delta\rho_n^2 P(Q) S(Q) \tag{1}$$

For dilute dispersions (where $S(Q) = 1$ and can be ignored), when $Q = 0$, $P(Q)$ is equal to 1, and the square root of the scattering intensity is proportional to the difference in SLD ($I(Q=0)^{1/2} \propto \Delta\rho_{\mathrm{n}}$).

$$I(Q=0) = \phi V_p \Delta\rho_{\mathrm{n}}^2 \tag{2}$$

By fixing the particle volume fraction and extrapolating the $Q = 0$ scattering intensity using the Guinier approximation [81], it is possible to experimentally determine the SLD of the latexes from the point where the solvent and particle have identical SLDs ($\Delta\rho_{\mathrm{n}} = 0$).

Figure 3 shows the measured values of the scattering intensity as a function of solvent SLD, which is varied by dispersing the latexes in mixtures of *n*-dodecane and *n*-dodecane-$d_{26}$. As expected, there is a linear relationship between $I(Q)^{1/2}$ and $\rho_{\mathrm{solvent}}$. The scattering intensity cannot be negative, and therefore, the experimental data is fit to the modulus or absolute value function. A fit to these data gives an SLD for the latexes of $\rho_{\mathrm{n}} = (1.1 \pm 0.1) \times 10^{-6}$ Å$^{-2}$. This is consistent with recent experimental measurements of the SLD of a similar PMMA latex [74] and the values used in other studies [58, 69, 70]. The scattering of the latexes has been analyzed using a model for core-shell spheres under different contrast conditions, and this confirmed that the scattering length density is higher in the center of the latex than in the stabilizer shell [73, 82, 83]. Given that the scattering length density of the whole latex is much more similar to the PMMA core than the PHSA stabilizer [58], for these dilute dispersions, it is reasonable to assume that the observed scattering intensity arises solely from the PMMA core.

Determining the SLD of the latexes enables the mass density of the particles ($\rho_m$) to be estimated. The SLD depends on the number of nuclei ($x_i$) each with a known coherent neutron scattering length ($b_i$) distributed across the molecular volume ($v_m$) [80].

$$\rho_m = \frac{\sum_i x_i b_i}{v_m} \tag{3}$$

Using the experimentally determined SLD ($\rho_{\mathrm{n}} = 1.1 \times 10^{-6}$ Å$^{-2}$) and assuming that the latex cores consist solely of PMMA ($(C_5O_2H_8)_n$), the mass density of the latexes is calculated to be $\rho_m = 1.176$ g cm$^{-3}$. This is less than the density of PMMA homopolymer (1.188 g cm$^{-3}$ [84]), which shows that the core of the latexes is similar to, yet not equivalent to, PMMA itself. This reduced density could be due to less efficient packing of polymer chains compared to the homopolymer, the presence of PHSA stabilizer in the core, or penetration of solvent into the core. If solvent in the core caused this reduction in density, it is possible to estimate the volume fraction of solvent that has penetrated into the latex cores using the mass density of

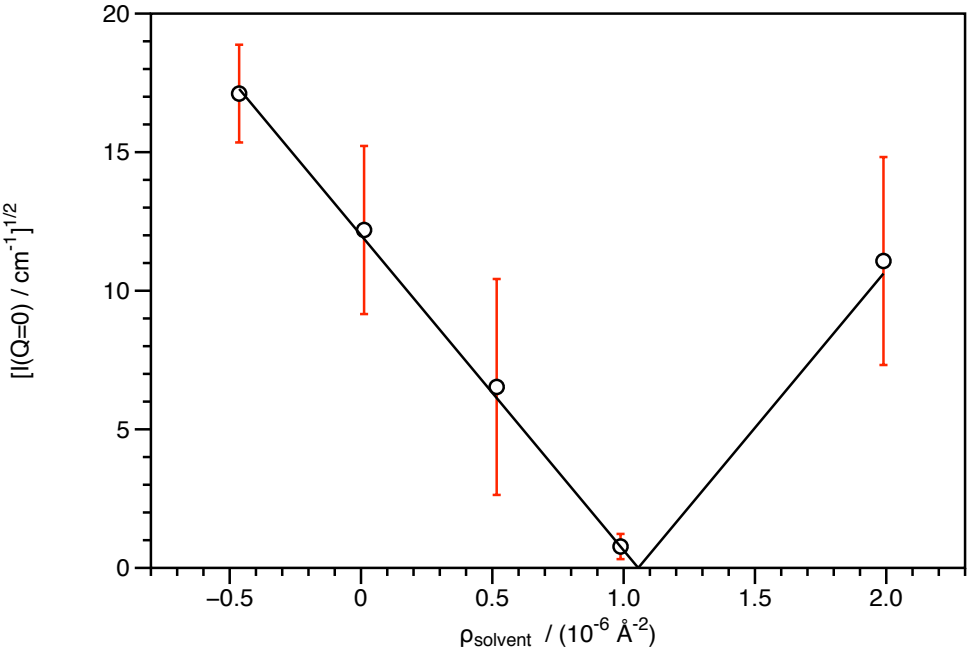


Figure 3: Experimental determination of the SLD of the 76 nm latexes. The scattering intensity ($I(Q)$) was measured for five dispersions at fixed volume fraction ($\phi = 0.02$) with different solvent SLDs ($\rho_{\text{solvent}}$). A linear fit to the data gives an SLD of $\rho_{\text{n}} = (1.1 \pm 0.1) \times 10^{-6}$ Å$^{-1}$.

PMMA homopolymer and the mass density of *n*-dodecane at this SLD. The amount of solvent in the cores, determined from this calculation, would be 0.03.

For the dilute dispersions, SANS intensity is dominated by scattering from the cores for several reasons. The SLD of the PHSA brushes ($\rho_{\text{PHSA}} = -0.06 \times 10^{-6}$ Å$^{-2}$) is similar to organic solvents ($\rho_{\text{dodecane}} = -0.43 \times 10^{-6}$ Å$^{-2}$), the SLD of the PMMA cores ($\rho_{\text{PMMA}} = 1.07 \times 10^{-6}$ Å$^{-2}$) is greater due its density, and the shell volume is occupied by a large amount of solvent. (Values of $\rho_{\text{n}}$ taken from Marković *et al.* [58].) The solvated latex shells, therefore, have little contrast with the solvent. For concentrated dispersions, however, the small contrast between the solvated PHSA brushes and the cores and the solvent results in detectable SANS intensity. SANS and SAXS measurements were performed on concentrated dispersions ($\phi \approx 0.2$) of 76 nm latexes in either unlabeled *n*-dodecane (SAXS) or latex contrast-matched *n*-dodecane (SANS), shown in Figure 4. The latex SLD was assumed to consist solely of the PMMA cores. The SAXS intensity arises from scattering of the cores only, as the stabilizer polymers have the same electron density as the solvent. Therefore, if the SANS contrast-matching to the cores is perfect, there should be detectable SAXS intensity and no detectable SANS intensity. As can be seen in Figure 4, this is not the case. There is measurable SANS intensity despite the solvent having the same SLD as the contrast-match point determined in Figure 3. It must, therefore, be due to the core-shell nature of the latexes. The PHSA chains have a different SLD than the PMMA cores, and when the scattering from the PMMA cores is suppressed, scattering intensity

is measured due to contrast between the solvated PHSA shells, the PMMA cores, and the solvent. Because the PMMA cores dominate at most solvent SLDs, this can only be observed near the contrast-match point.

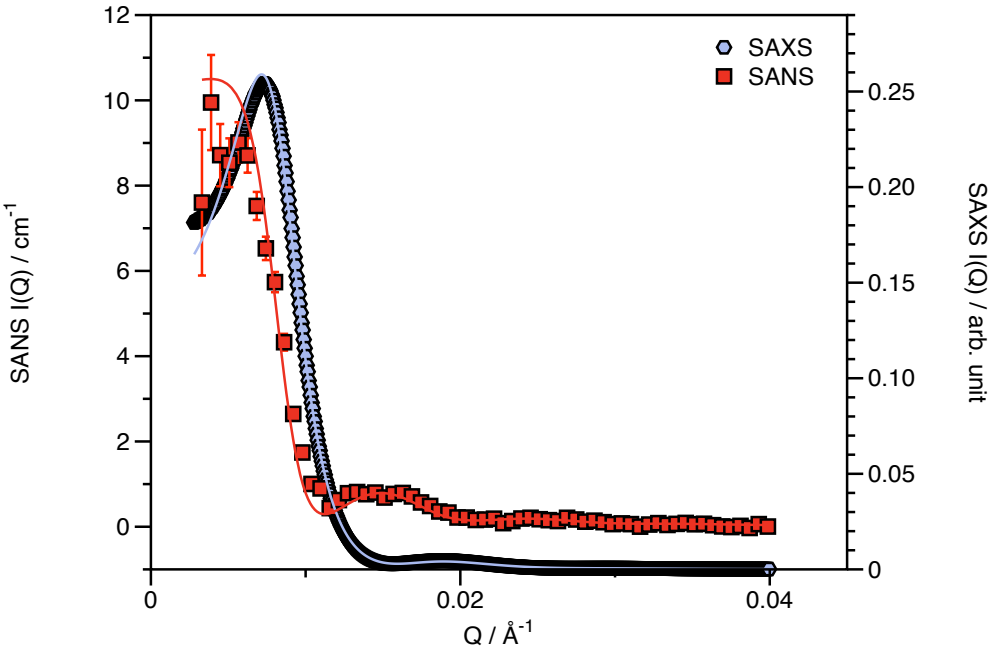


Figure 4: SANS and SAXS measurements conducted on concentrated dispersions ($\phi \approx 0.2$) of 76 nm latexes in $n$-dodecane (SAXS) and latex contrast-matched $n$-dodecane (SANS). Both are fit to a concentric sphere form factor [51, 85] with a core radius of 27.9 nm and a shell thickness of 6 nm, including a hard sphere structure factor [86]. The difference in the profiles of the two curves originates from a contribution to the SANS intensity from the PHSA polymer in the stabilizer shells.

Both raw scattering SAXS and SANS data along with model fits to a concentric sphere form factor [51, 85] with a hard-sphere structure factor [86] are shown in Figure 4. The concentric sphere form factor is used in accordance [51, 70, 85] with literature to account for any scattering from the PHSA stabilizer shells and to set the radius for the hard-sphere structure factor to that of the whole latex (core radius plus shell thickness). As concentrated dispersions are now studied (unlike the dilute dispersions used for the data in Figure 3), there is an $S(Q)$ contribution to the scattering curve. The radii of the cores are determined from fitting to the SAXS data from the concentrated dispersion, and the thicknesses of the PHSA shells are set to 6 nm, which is the value used by Marković *et al.* [58].

The SAXS data are useful for studying the interaction of the latexes, and as can be seen, the data are well fit using a hard-sphere $S(Q)$, which is gratifying given their use as model spheres. The hard-sphere volume fraction, which determines the profile of the $S(Q)$ curve, is greater than the anticipated volume fraction by $\sim 10\%$ ($\phi_{\text{fit}} = 0.21$). Defining and determining the volume fraction of these latexes is known to be a challenging problem [87]. The anticipated volume fractions are determined by mass loss, and it is not surprising that the real volume fraction would therefore be greater. The mean radius and size distribution are allowed to vary to best fit the data, and the best fit radius ($r = 27.9$ nm with $\sigma = 0.12$) matches the

dilute case well and is less than the solvodynamic radius, emphasizing that SAXS intensity arises exclusively from the latex cores.

The SANS curve in Figure 4 is qualitatively different to the SAXS curve. As the SLD of the solvent is matched to the particle SLD determined in Figure 3, there should be no residual scattering. This is indeed the case for a dilute dispersion of 76 nm latexes in contrast-matched *n*-dodecane, but the data in Figure 4 show that there is scattering from a concentrated dispersion. (Scattering curves comparing the two dispersions in latex contrast-matched solvent are shown in the Electronic Supporting Information.) If the residual SANS intensity was due to the PMMA cores of the latexes, then the profiles of the SAXS and SANS curves should be identical. Since they are not, this indicates that the additional intensity must come from the shells of the latexes. This makes sense, given that the curve shifts to lower-$Q$, corresponding to a larger size. The difference in the peak in the hard-sphere $S(Q)$ is different for the SANS data due to use of a core-shell form factor and the scattering from the shell, rather than the core, dominating

To model the SANS data, the dispersion is assumed to be identical to the dispersion measured by SAXS, as the only difference between the two is the isotopic-labeling of the solvent. Therefore, the differences between the scattering curves are due solely to different values for the SLDs. The shell thickness (6 nm), the core radius (27.9 nm), and the size distribution ($\sigma = 0.12$) are fixed. The solvent SLD is set to the value known from sample preparation ($\rho_{\text{solvent}} = 1.16 \times 10^{-6}$ Å$^{-2}$) rather than the fit core SLD ($\rho_{\text{core}} = 1.1 \times 10^{-6}$ Å$^{-2}$) as the high particle concentration means that a small contrast mismatch could result in detectable scattering. The SLD of the shells was initially set to the value of pure PHSA used in the literature ($\rho_{\text{shell}} = -0.06 \times 10^{-6}$ Å$^{-2}$ [51, 58]). When these values are chosen, the scattering intensity is much greater than that measured experimentally. In order to fit the data, the size dimensions are fixed, and all SLDs are allowed to vary. This gives a good fit to the data, as shown in Figure 4. The values of $\rho_{\text{solvent}}$ and $\rho_{\text{core}}$ do not vary significantly ($< 5\%$), but the change in $\rho_{\text{shell}}$ is significant. It increases to $0.96 \times 10^{-6}$ Å$^{-2}$. This greatly reduces $\Delta\rho_{\text{n}}$ between the shells and both the cores and the solvent, but it does not reduce it to zero. This is the origin of the residual scattering in Figure 4. If the SLD of the shells is assumed to consist of scattering from the polymer as well as penetrated solvent, then this gives a solvent volume fraction in the stabilizer shells of 0.83. In the SANS study of this concentrated dispersion of latexes, data cannot be fit if the SLD of the shells is set to that of the PHSA homopolymer as reported previously [51, 58], but they also cannot be fit if the scattering from PHSA is ignored (assuming completely solvated shells with no scattering from the PHSA brushes).

### *3.3. 685 nm diameter latexes*

Analytical centrifugation can be used to study large ($> 100$ nm) latexes. This technique has been infrequently used to study PMMA latexes; the only reports in the literature use the technique to study dense colloidal fluids [88] or the density of nanoparticle-containing latexes [89]. This study provides a rare

example of how this technique can be used with polymer colloids in nonpolar solvents.

The internal structure of the large 685 nm latexes cannot be studied using SANS as their size is much greater than that the $Q$-range of conventional SANS instrumentation (typically $10^{-3}$–$10^{-1}$ Å$^{-1}$) [90], although the particle surfaces could be studied over this lengthscale. Such length-scales can be studied using ultra small-angle neutron scattering (USANS) [80, 90, 91], but these measurements cause other difficulties. Due to the greater scattering intensities ($I(Q) \propto V_p^2 \propto r_p^6$), any difference from the anticipated solvent SLD caused by sample preparation would result in considerable scattering intensity. Also, given the density difference between the particle and solvent, particles could sediment during the experiment.

Analytical centrifugation is a method that can be used to study the particles; it is a well-known way to study the size and density of colloids [92]. However, the approach has predominantly been employed in water, due to application in the study of biomolecules [93, 94]. Growney *et al.* recently used the technique to study polymer-stabilized carbon black particles in $n$-alkanes, which shows its versatility in nonpolar solvents as well [95–97]. To enable more precise determination of colloidal properties, sedimentation measurements can be performed in isotopically-labeled solvents, which are chemically identical but differ in fluid properties. This has been done with $H_2O$ and $D_2O$ [98, 99], but similar experiments can be conducted with any pair of solvents that are chemically similar but of different densities and viscosities.

The sedimentation velocities of 685 nm latexes dispersed in both $n$-dodecane and deuterium-labeled $n$-dodecane-$d_{26}$ have been measured using the LUMiSizer instrument. A consequence of isotopically-labeling the solvent is that both the fluid density and viscosity are different, and the physical properties of the two solvents are shown in Table 2. The densities of the two solvents are known [100]. The viscosity of $n$-dodecane was taken from the literature and that for $n$-dodecane-$d_{26}$ was calculated using an empirical mathematical relationship between molar mass and viscosity for isotopically-labeled compounds: the viscosity is proportional to the square root of the molar mass [101, 102].

Table 2: Physical properties of $n$-dodecane and $n$-dodecane-$d_{26}$

| Solvent | Density / (g cm$^{-3}$) [100] | Viscosity / ($10^{-3}$ Pa·s) [101, 102] |
|---|---|---|
| $n$-Dodecane | 0.75 | 1.383 |
| $n$-Dodecane-$d_{26}$ | 0.864 | 1.485 |

The analytical centrifugation data were processed using LUMiSizer software to determine the sedimentation velocity of the particles. (Raw data from the LUMiSizer measurements are shown in the Supporting Information.) The particles sediment completely during the course of the measurements in both solvents, and the sedimentation fronts do not diverge with time, indicating that the particle size distribution is relatively narrow. Due to the differing densities and viscosities of the solvents, the sedimentation velocities are indeed different (7.7 $\mu$m s$^{-1}$ in $n$-dodecane and 5.2 $\mu$m s$^{-1}$ in $n$-dodecane-$d_{26}$).

For spheres of uniform composition, the particle density can be calculated from the properties of the fluid

(viscosity $\eta$ and mass density $\rho$) and the particle velocity ($v$) for measurements performed in unlabeled and deuterium-labeled solvents [92]. This simple approach, however, is not strictly appropriate for the concentric spheres used in this study. The density cannot be averaged over the particle, as the core and shell densities differ. Also, the different densities of the two solvents mean that the densities of the shells, which were shown in Section 3.2 to be considerably solvated, differ in the two cases, whereas the density of the cores stay the same.

To determine the particle density for spheres of uniform composition, the radii of the particles in the two solvents are taken to be equal, and the same approach can be taken for concentric spheres. In this case, the composite particle densities are now size dependent (due to the ratio of the volume of the cores to the total volume), and the shell densities differ in the two solvents (due to the different densities of *n*-dodecane and *n*-dodecane-$d_{26}$). The shell densities ($\rho_{s,\mathrm{H}}$ in *n*-dodecane and $\rho_{s,\mathrm{D}}$ in *n*-dodecane-$d_{26}$) can be determined from the density of the brush polymer ($\rho_s$), the density of the fluid ($\rho_{\mathrm{H}}$ for *n*-dodecane and $\rho_{\mathrm{D}}$ for *n*-dodecane-$d_{26}$), and the volume fraction of the shell volume occupied by solvent ($\phi_f$).

$$\rho_{s,\mathrm{H}} = \phi_f \rho_{\mathrm{H}} + (1 - \phi_f)\, \rho_s \tag{4}$$

$$\rho_{s,\mathrm{D}} = \phi_f \rho_{\mathrm{D}} + (1 - \phi_f)\, \rho_s \tag{5}$$

The dimensions of the particle, the core radius $r_c$ and the total radius $r_s$, as well as the volume fraction of solvent in the shells ($\phi_f$) are known, from measurements discussed in Sections 3.1 and 3.2. Using these values together with the sedimentation velocities calculated from the LUMiSizer, it is possible to calculate the density of the cores ($\rho_c$) unambiguously using Equation 6.

$$\rho_c = r_c^3 \left[(\eta_{\mathrm{H}} v_{\mathrm{H}} - \eta_{\mathrm{D}} v_{\mathrm{D}})\right]^{-1} \times \left[(\eta_{\mathrm{D}} v_{\mathrm{D}}) \left[\left(r_s^3 - r_c^3\right) \rho_{s,\mathrm{H}} - \rho_{\mathrm{H}} r_s^3\right] - (\eta_{\mathrm{H}} v_{\mathrm{H}}) \left[\left(r_s^3 - r_c^3\right) \rho_{s,\mathrm{D}} - \rho_{\mathrm{D}} r_s^3\right]\right] \tag{6}$$

PHSA shell thicknesses in the literature range from 6 nm to 19 nm, depending on the solvent, the batch of particles, and technique used to study them [51, 58, 79]. As the same batch of PHSA stabilizer was used to prepare both the 76 and 685 nm latexes, the values of the shell thickness (6 nm) and $\phi_f$ (0.83) calculated in Section 3.2 were used to solve Equation 6. This gives a core density of $\rho_c = 1.173$ g cm$^{-3}$. This value is gratifyingly similar to that determined for the 76 nm latexes. The volume fraction of solvent that has penetrated into the cores can be estimated from the density of the cores, as was done from the CV-SANS determined mass density of the 76 nm latexes, although strictly if solvent penetration were responsible for the reduction in density, then the core densities would be different for the two solvents. However, the volume fraction occupied by solvent is small, and so if this were the case, the difference in core densities would be very small. Using the density of *n*-dodecane to perform this calculation gives a fraction of solvent in the cores of 0.04.

Having determined the density of the latex cores, it is possible to calculate the composite density of the entire sterically-stabilized particles. This is a sum of the volume fraction weighted densities of all species

that make up the particle (PMMA cores, PHSA stabilizer, and associated solvent). The composite density of the latexes in *n*-dodecane is 1.146 g cm$^{-3}$ and in *n*-dodecane-$d_{26}$ is 1.153 g cm$^{-3}$. These are lower than the core density due to the solvent associated with the stabilizer shell. This composite density was used to determine particle size distributions from the LUMiSizer data, and the results are shown in Figure 5 along with the volume-weighted DLS distribution. The LUMiSizer data were fit to a log-normal distribution. The radii and widths of the distributions determined from this fit are $r = 333$ nm and $\sigma = 0.03$ for *n*-dodecane and $r = 330.$ nm and $\sigma = 0.05$ for *n*-dodecane-$d_{26}$. The data from the LUMiSizer are very similar, despite the differing solvents. On the other hand, if the density of PMMA homopolymer is used for these calculations rather than the correct composite density, the calculated particle sizes are much too low. This emphasizes the importance of treating the particles as concentric spheres with highly solvated stabilizer shells.

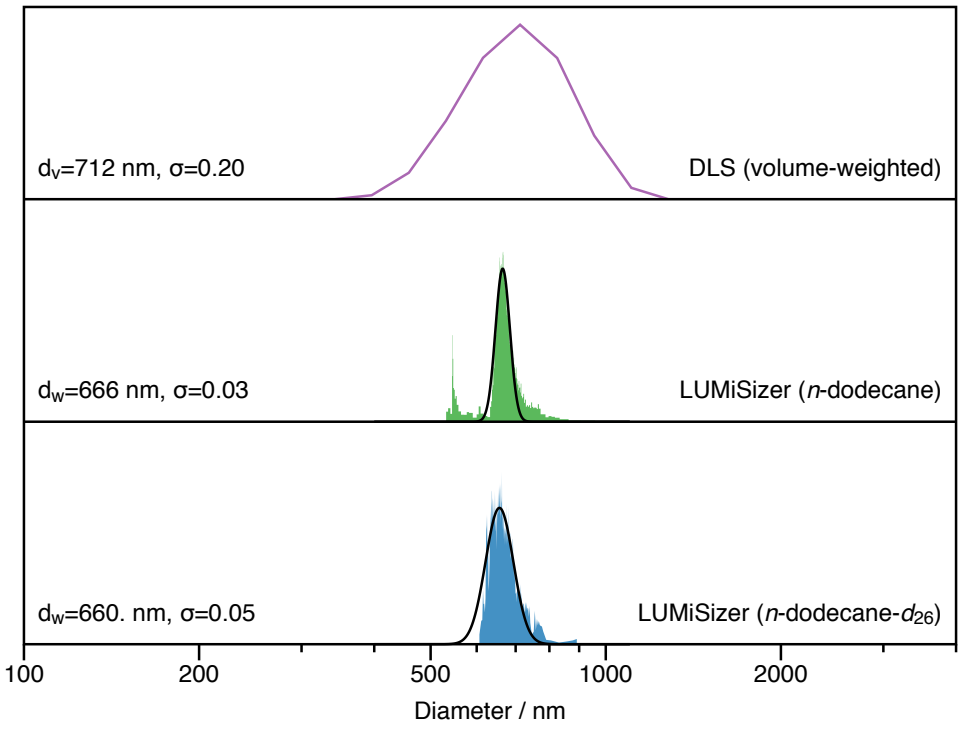


Figure 5: Size distributions for 685 nm latexes measured using DLS and the LUMiSizer. The LUMiSizer gives a mass-weighted distribution, which can be compared to the DLS volume-weighted distribution. The LUMiSizer centrifugation profiles were fit using composite densities calculated for the latexes and solvent densities and viscosities appropriate to the isotopic labeling, as explained in the text. The radii of the latexes in the two solvents are found to be essentially equal and consistent with the size determined from DLS.

## 4. Discussion

The results discussed in the previous sections have enabled the internal structure of the latexes to be examined. Properties of interest for both latexes as well as PMMA homopolymer are shown in Table 3. SANS has enabled the density of the PMMA cores ($\rho_m$) and the solvation of the PHSA shells ($\phi_f$) of the

76 nm latexes to be determined. Analytical centrifugation has enabled the size of the latexes as well as the density of the PMMA cores ($\rho_m$) to be determined.

Table 3: Solvation and Density of PMMA latexes

| Latex | Method | Shell solvation ($\phi_f$) |
|---|---|---|
| 76 nm | Concentrated SANS | 0.83 |
| 685 nm | Centrifugation | 0.83[a] |

| Latex | Method | Core density, $\rho_m$ / (g cm$^{-3}$) |
|---|---|---|
| 76 nm | CV-SANS | 1.176 |
| 685 nm | Centrifugation | 1.173 |
| PMMA homopolymer | Literature[b] | 1.188 |

[a] Set to value determined for 76 nm latexes
[b] Value from Gall and McCrum [84].

The experimentally determined densities of the PMMA cores of the latexes are similar to that of PMMA homopolymer [84] rather than a mix of PHSA and PMMA. This shows that the PHSA stabilizer chains are predominantly segregated to the edge of the latexes. The similarity of the core density of the latexes to that of pure PMMA is also interesting given previous experiments on such colloids. The densities of the cores can be estimated to be essentially equivalent PMMA polymer with either a small amount of solvent penetration ($\sim 0.03$) or a slight expansion. Fluorescence energy-transfer studies have shown that small molecules can distribute throughout the cores [103–105]. Other small molecules, such as residual hexane solvent [106] or surfactant charging agents [74, 76], can also be distributed throughout the cores of the latexes. Given that molecules are able to partition throughout the volume of the latexes, the core polymers could be highly porous and therefore significantly less dense than the pure polymer. It appears that only a small reduction in density is required; the volume that molecules can partition through is small.

The solvation of the shells these latexes in *n*-dodecane is also gratifyingly similar to that determined by Washington *et al.* using SESANS [79]. Both values are determined using different neutron scattering methods (either SESANS or CV-SANS) but different solvents. The fact that two different approaches give similar values for the fraction of solvent in the stabilizer shells of similar, yet not identical, systems gives confidence to the values obtained and shows that PHSA shells are solubilized similarly by different hydrocarbon solvents. The shells of these latexes are highly solvated but cannot be thought of as equivalent to either the solvent or the PHSA homopolymer. The detectable scattering intensity shown in Figure 4, seen for concentrated dispersions but of too low intensity to be seen for dilute dispersions, must be carefully considered and accounted for when interpreting neutron scattering data from these latexes.

## 5. Conclusions

PMMA latexes are frequently used as model physical particles, and in this study, both small-angle scattering and analytical centrifugation measurements show that considering them as effective hard spheres is appropriate. That these types of latexes interact as essentially hard spheres is known from small-angle scattering [58, 77] and confocal microscopy [31–33] measurements, in particular, but there have been few studies into the internal structure of the cores [106] and the amount of solvent contained in the stabilizer [79]. Comparing results using different latexes is challenging as the particles will have been prepared by different groups, and the synthesis of the PHSA stabilizer is known to be variable [38]. By studying latexes of different sizes that are prepared using the same batches of reagents, it is possible to directly determine the intrinsic, size-independent internal structure of these latexes and to isolate any differences that are due solely to the size.

The high resolution of modern scattering and centrifugation instrumentation has revealed information about the internal structure in greater detail than possible before. The experiments performed in this study show that, regardless of the size of the latexes, their core densities are similar to, though slightly lower than, that of PMMA homopolymer and their shells are highly solvated ($\sim 85\%$ by volume). These properties are found to be independent of the particle size. The approach used to study these two latexes dispersed in *n*-dodecane is a promising method for characterizing the internal structure of latexes in nonaqueous solvents generally, and it could be extended to other solvents or mixtures of solvents as required for other experiments or applications.

This has consequences for correctly interpreting experiments using such latexes as well as sterically-stabilized colloids in nonpolar solvents generally. As an example, when using these particles to study charged sphere interactions or the depletion potential, autoionizable solvents [42, 43], charging agents [10, 46–48, 50], or non-adsorbing polymers [45] are added. Introducing additional solutes to the dispersions further complicates an already complex system. Without an appreciation of the chemical composition and internal structure of the latexes, the distribution of these added components cannot be known. This is particularly true when interpreting data from neutron scattering experiments on dispersions of these latexes [51, 58, 67–74, 76, 79], where the contrast between the polymer and isotopically-labeled solvents may be significant. Neglecting this interaction could lead to incorrect interpretations of the scattering data. As an example, in dilute dispersions, the small amount of scattering from the PHSA shells is not significant in contrast-matched solvent [73, 74], whereas in concentrated dispersions, whether in contrast-matched solvent or for SESANS measurements [79], the scattering from the stabilizer shells can be significant. The results in this study show how complementary structural information of colloids of different sizes in nonpolar solvents can be obtained. Regardless of the technique used to study the properties of the colloids, the structural detail presented is expected to aid the accurate interpretation of measurements of academically and technologically interesting

dispersions in nonpolar solvents in the future.


## Acknowledgements

GNS and DAJG acknowledge Merck Chemicals Ltd. UK, an affiliate of Merck KGaA, Darmstadt, Germany, and the UK Engineering and Physical Sciences Research Council (EPSRC) for the provision of a CASE PhD studentship. The authors thank the UK Science and Technology Facilities Council (STFC) for allocation of beamtime and Xpress experiments at ISIS and grants toward consumables and travel. The authors thank Diamond Light Source for provision of beamtime on I22 and travel funding. This work benefitted from SasView software, originally developed by the DANSE project under NSF award DMR-0520547. Prof. Patrick W. Fowler and Dr. David J. Growney (University of Sheffield) are acknowledged for useful discussions. Jonathan Jones (Electron and Scanning Probe Microscopy Facility, University of Bristol) is acknowledged for scanning electron microscopy (SEM) images.


## References


[1] H.-F. Eicke, Micelles, Springer, Berlin, Heidelberg, 1980, Ch. Surfactants in nonpolar solvents, pp. 85–145. doi:10.1007/BFb0048489.

[2] J. Eastoe, B. H. Robinson, D. C. Steytler, D. Thorn-Leeson, Structural studies of microemulsions stabilised by aerosol-OT, Adv. Colloid Interface Sci. 36 (1991) 1–31. doi:10.1016/0001-8686(91)80027-H.

[3] T. K. De, A. Maitra, Solution behaviour of Aerosol OT in non-polar solvents, Adv. Colloid Interface Sci. 59 (1995) 95–193. doi:10.1016/0001-8686(95)80005-N.

[4] V. Novotny, Applications of nonaqueous colloids, Colloids Surf. 24 (4) (1987) 361–375. doi:10.1016/0166-6622(87)80241-X.

[5] I. D. Morrison, Electrical charges in nonaqueous media, Colloids Surf. A: Physicochem. Eng. Aspects 71 (1) (1993) 1–37. doi:10.1016/0927-7757(93)80026-B.

[6] J. Eastoe, M. J. Hollamby, L. Hudson, Recent advances in nanoparticle synthesis with reversed micelles, Adv. Colloid Interface Sci. 128–130 (2006) 5–15. doi:10.1016/j.cis.2006.11.009.

[7] L. Hudson, J. Eastoe, P. Dowding, Nanotechnology in action: Overbased nanodetergents as lubricant oil additives, Adv. Colloid Interface Sci. 123–126 (2006) 425–431. doi:10.1016/j.cis.2006.05.003.

[8] A. P. Richez, H. N. Yow, S. Biggs, O. J. Cayre, Dispersion polymerization in non-polar solvent: Evolution toward emerging applications, Prog. Polym. Sci. 38 (6) (2013) 897–931. doi:10.1016/j.progpolymsci.2012.12.001.

[9] G. N. Smith, J. Eastoe, Controlling colloid charge in nonpolar liquids with surfactants, Phys. Chem. Chem. Phys. 15 (2) (2013) 424–439. doi:10.1039/c2cp42625k.

[10] G. N. Smith, J. E. Hallett, J. Eastoe, Celebrating *Soft Matter*'s 10th Anniversary: Influencing the charge of poly(methyl methacrylate) latexes in nonpolar solvents, Soft Matter 11 (41) (2015) 8029–8041. doi:10.1039/C5SM01190F.

[11] M. M. Gacek, J. C. Berg, The role of acid–base effects on particle charging in apolar media, Adv. Colloid Interface Sci. 220 (2015) 108–123. doi:10.1016/j.cis.2015.03.004.

[12] M. J. Derry, L. A. Fielding, S. P. Armes, Polymerization-induced self-assembly of block copolymer nanoparticles via RAFT non-aqueous dispersion polymerization, Prog. Polym. Sci. 52 (2016) 1–18. doi:10.1016/j.progpolymsci.2015.10.002.

[13] A. Klinkenberg, J. L. van der Minne (Eds.), Electrostatics in the Petroleum Industry: The Prevention of Explosion Hazards, Elsevier, London, 1958.

[14] A. Jukic, E. Vidovic, Z. Janovic, Alkyl methacrylate and styrene terpolymers as lubricating oil viscosity index improvers, Chem. Technol. Fuels Oils 43 (5) (2007) 386–394. doi:10.1007/s10553-007-0068-9.

[15] R. Zheng, G. Liu, M. Devlin, K. Hux, T.-C. Jao, Friction reduction of lubricant base oil by micelles and crosslinked micelles of block copolymers, Tribol. Trans. 53 (1) (2009) 97–107. doi:10.1080/10402000903226390.

[16] H. Block, J. P. Kelly, Electro-rheology, J. Phys. D: Appl. Phys. 21 (12) (1988) 1661–1677. URL `http://stacks.iop.org/0022-3727/21/i=12/a=001`

[17] A. P. Gast, C. F. Zukoski, Electrorheological fluids as colloidal suspensions, Adv. Colloid Interface Sci. 30 (1989) 153–202. doi:10.1016/0001-8686(89)80006-5.

[18] I. Ota, J. Ohnishi, M. Yoshiyama, Electrophoretic image display (EPID) panel, Proc. IEEE 61 (7) (1973) 832–836. doi:10.1109/PROC.1973.9173.

[19] B. Comiskey, J. D. Albert, H. Yoshizawa, J. Jacobson, An electrophoretic ink for all-printed reflective electronic displays, Nature 394 (6690) (1998) 253–255. doi:10.1038/28349.

[20] J. Heikenfeld, P. Drzaic, J.-S. Yeo, T. Koch, Review paper: A critical review of the present and future prospects for electronic paper, J. Soc. Info. Display 19 (2) (2011) 129–156. doi:10.1889/JSID19.2.129.

[21] S. Klein, Electrophoretic liquid crystal displays: how far are we?, Liq. Cryst. Rev. 1 (1) (2013) 52–64. doi:10.1080/21680396.2013.786246.
[22] R. J. R. Cairns, R. H. Ottewill, D. W. J. Osmond, I. Wagstraff, Studies on the preparation and properties of latices in nonpolar media, J. Colloid Interface Sci. 54 (1) (1976) 45–51. doi:10.1016/0021-9797(76)90283-6.
[23] L. Antl, J. W. Goodwin, R. D. Hill, R. H. Ottewill, S. M. Owens, S. Papworth, J. A. Waters, The preparation of poly(methyl methacrylate) latices in non-aqueous media, Colloids Surf. 17 (1) (1986) 67–78. doi:10.1016/0166-6622(86)80187-1.
[24] S. M. Klein, V. N. Manoharan, D. J. Pine, F. F. Lange, Preparation of monodisperse PMMA microspheres in nonpolar solvents by dispersion polymerization with a macromonomeric stabilizer, Colloid Polym. Sci. 282 (1) (2003) 7–13. doi:10.1007/s00396-003-0915-0.
[25] H. V. Harris, S. J. Holder, Octadecyl acrylate based block and random copolymers prepared by ATRP as comb-like stabilizers for colloidal micro-particle one-step synthesis in organic solvents, Polymer 47 (16) (2006) 5701–5706. doi:10.1016/j.polymer.2006.06.011.
[26] H. V. Penfold, S. J. Holder, B. E. McKenzie, Octadecyl acrylate – Methyl methacrylate block and gradient copolymers from ATRP: Comb-like stabilizers for the preparation of micro- and nano-particles of poly(methyl methacrylate) and poly(acrylonitrile) by non-aqueous dispersion polymerization, Polymer 51 (9) (2010) 1904–1913. doi:10.1016/j.polymer.2010.02.029.
[27] A. P. Richez, L. Farrand, M. Goulding, J. H. Wilson, S. Lawson, S. Biggs, O. J. Cayre, Poly(dimethylsiloxane)-stabilized polymer particles from radical dispersion polymerization in nonpolar solvent: Influence of stabilizer properties and monomer type, Langmuir 30 (5) (2014) 1220–1228. doi:10.1021/la4039304.
[28] K. E. Belsey, C. Topping, L. D. Farrand, S. J. Holder, Inhibiting the thermal gelation of copolymer stabilized nonaqueous dispersions and the synthesis of full color PMMA particles, Langmuir 32 (11) (2016) 2556–2566. doi:10.1021/acs.langmuir.6b00063.
[29] P. N. Pusey, W. van Megen, Phase behaviour of concentrated suspensions of nearly hard colloidal spheres, Nature 320 (6060) (1986) 340–342. doi:10.1038/320340a0.
[30] P. N. Pusey, W. van Megen, Observation of a glass transition in suspensions of spherical colloidal particles, Phys. Rev. Lett. 59 (18) (1987) 2083–2086. doi:10.1103/PhysRevLett.59.2083.
[31] E. R. Weeks, J. C. Crocker, A. C. Levitt, A. Schofield, D. A. Weitz, Three-dimensional direct imaging of structural relaxation near the colloidal glass transition, Science 287 (5453) (2000) 627–631. doi:10.1126/science.287.5453.627.
[32] U. Gasser, E. R. Weeks, A. Schofield, P. N. Pusey, D. A. Weitz, Real-space imaging of nucleation and growth in colloidal crystallization, Science 292 (5515) (2001) 258–262. doi:10.1126/science.1058457.
[33] A. Yethiraj, A. van Blaaderen, A colloidal model system with an interaction tunable from hard sphere to soft and dipolar, Nature 421 (6922) (2003) 513–517. doi:10.1038/nature01328.
[34] D. Reinke, H. Stark, H.-H. von Grünberg, A. B. Schofield, G. Maret, U. Gasser, Noncentral forces in crystals of charged colloids, Phys. Rev. Lett. 98 (3) (2007) 038301. doi:10.1103/PhysRevLett.98.038301.
[35] C. Pathmamanoharan, C. Slob, H. N. W. Lekkerkerker, Preparation of polymethylmethacrylate latices in non-polar media, Colloid Polym. Sci. 267 (5) (1989) 448–450. doi:10.1007/BF01410191.
[36] C. Pathmamanoharan, K. Groot, J. K. G. Dhont, Preparation and characterization of crosslinked PMMA latex particles stabilized by grafted copolymer, Colloid Polym. Sci. 275 (9) (1997) 897–901. doi:10.1007/s003960050164.
[37] G. Bosma, C. Pathmamanoharan, E. H. A. de Hoog, W. K. Kegel, A. van Blaaderen, H. N. W. Lekkerkerker, Preparation of monodisperse, fluorescent PMMA–latex colloids by dispersion polymerization, J. Colloid Interface Sci. 245 (2) (2002) 292–300. doi:10.1006/jcis.2001.7986.
[38] M. T. Elsesser, A. D. Hollingsworth, Revisiting the synthesis of a well-known comb-graft copolymer stabilizer and its application to the dispersion polymerization of poly(methyl methacrylate) in organic media, Langmuir 26 (23) (2010) 17989–17996. doi:10.1021/la1034917.
[39] M. T. Elsesser, A. D. Hollingsworth, K. V. Edmond, D. J. Pine, Large core–shell poly(methyl methacrylate) colloidal clusters: Synthesis, characterization, and tracking, Langmuir 27 (3) (2011) 917–927. doi:10.1021/la1034905.
[40] P. N. Pusey, W. van Megen, P. Bartlett, B. J. Ackerson, J. G. Rarity, S. M. Underwood, Structure of crystals of hard colloidal spheres, Phys. Rev. Lett. 63 (25) (1989) 2753–2756. doi:10.1103/PhysRevLett.63.2753.
[41] C. P. Royall, W. C. K. Poon, E. R. Weeks, In search of colloidal hard spheres, Soft Matter 9 (1) (2013) 17–27. doi:10.1039/C2SM26245B.
[42] M. E. Leunissen, C. G. Christova, A.-P. Hynninen, C. P. Royall, A. I. Campbell, A. Imhof, M. Dijkstra, R. van Roij, A. van Blaaderen, Ionic colloidal crystals of oppositely charged particles, Nature 437 (7056) (2005) 235–240. doi:10.1038/nature03946.
[43] P. Bartlett, A. I. Campbell, Three-dimensional binary superlattices of oppositely charged colloids, Phys. Rev. Lett. 95 (12) (2005) 128302. doi:10.1103/PhysRevLett.95.128302.
[44] S. M. Ilett, A. Orrock, W. C. K. Poon, P. N. Pusey, Phase behavior of a model colloid-polymer mixture, Phys. Rev. E 51 (2) (1995) 1344–1352. doi:10.1103/PhysRevE.51.1344.
[45] W. C. K. Poon, The physics of a model colloid–polymer mixture, J. Phys.: Condens. Matter 14 (33) (2002) R859–R880. URL http://stacks.iop.org/0953-8984/14/i=33/a=201
[46] M. F. Hsu, E. R. Dufresne, D. A. Weitz, Charge stabilization in nonpolar solvents, Langmuir 21 (11) (2005) 4881–4887. doi:10.1021/la046751m.
[47] G. S. Roberts, R. Sanchez, R. Kemp, T. Wood, P. Bartlett, Electrostatic charging of nonpolar colloids by reverse micelles, Langmuir 24 (13) (2008) 6530–6541. doi:10.1021/la703908n.
[48] R. Sánchez, P. Bartlett, Synthesis of charged particles in an ultra-low dielectric solvent, Soft Matter 7 (3) (2011) 887–890.

doi:10.1039/C0SM01454K.
URL http://dx.doi.org/10.1039/C0SM01454K
[49] F. Beunis, F. Strubbe, K. Neyts, D. Petrov, Beyond Millikan: The dynamics of charging events on individual colloidal particles, Phys. Rev. Lett. 108 (1) (2012) 016101. doi:10.1103/PhysRevLett.108.016101.
[50] D. A. J. Gillespie, J. E. Hallett, O. Elujoba, A. F. Che Hamzah, R. M. Richardson, P. Bartlett, Counterion condensation on spheres in the salt-free limit, Soft Matter 10 (4) (2014) 566–577. doi:10.1039/C3SM52563E.
[51] D. J. Cebula, J. W. Goodwin, R. H. Ottewill, G. Jenkin, J. Tabony, Small angle and quasi-elastic neutron scattering studies on polymethylmethacrylate latices in nonpolar media, Colloid Polym. Sci. 261 (7) (1983) 555–564. doi:10.1007/BF01526620.
[52] L. Palangetic, K. Feldman, R. Schaller, R. Kalt, W. Caseri, J. Vermant, From near hard spheres to colloidal surfboards, Faraday Discuss.doi:10.1039/C6FD00052E.
[53] M. N. van der Linden, J. C. P. Stiefelhagen, G. Heessels-Gürboğa, J. E. S. van der Hoeven, N. A. Elbers, M. Dijkstra, A. van Blaaderen, Charging of poly(methyl methacrylate) (PMMA) colloids in cyclohexyl bromide: Locking, size dependence, and particle mixtures, Langmuir 31 (1) (2015) 65–75. doi:10.1021/la503665e.
[54] R. H. Ottewill, I. Livsey, The imbibition of carbon disulphide by poly(methyl methacrylate) latex particles, Polymer 28 (1) (1987) 109 – 113. doi:10.1016/0032-3861(87)90324-7.
[55] C. P. Royall, M. E. Leunissen, A. van Blaaderen, A new colloidal model system to study long-range interactions quantitatively in real space, J. Phys.: Condens. Matter 15 (48) (2003) S3581–S3596. doi:10.1088/0953-8984/15/48/017.
[56] S.-E. Phan, W. B. Russel, Z. Cheng, J. Zhu, P. M. Chaikin, J. H. Dunsmuir, R. H. Ottewill, Phase transition, equation of state, and limiting shear viscosities of hard sphere dispersions, Phys. Rev. E 54 (6) (1996) 6633–6645. doi:10.1103/PhysRevE.54.6633.
[57] R. P. A. Dullens, E. M. Claesson, W. K. Kegel, Preparation and properties of cross-linked fluorescent poly(methyl methacrylate) latex colloids, Langmuir 20 (3) (2004) 658–664. doi:10.1021/la035729a.
[58] I. Marković, R. H. Ottewill, S. M. Underwood, T. F. Tadros, Interactions in concentrated nonaqueous polymer latices, Langmuir 2 (5) (1986) 625–630. doi:10.1021/la00071a018.
[59] S. L. Gras, A. M. Squires, Dried and hydrated x-ray scattering analysis of amyloid fibrils, in: A. F. Hill, K. J. Barnham, S. P. Bottomley, R. Cappai (Eds.), Protein Folding, Misfolding, and Disease, Vol. 752 of Methods in Molecular Biology, Humana Press, 2011, pp. 147–163. doi:10.1007/978-1-60327-223-0_10.
[60] T. Snow, Yax 2.0.
URL http://www.cunninglemon.com/projects.YAX.html
[61] Sasview for small angle scattering analysis.
URL http://www.sasview.org/
[62] R. K. Heenan, S. E. Rogers, D. Turner, A. E. Terry, J. Treadgold, S. M. King, Small angle neutron scattering using Sans2d, Neutron News 22 (2) (2011) 19–21. doi:10.1080/10448632.2011.569531.
[63] R. K. Heenan, J. Penfold, S. M. King, SANS at pulsed neutron sources: Present and future prospects, J. Appl. Cryst. 30 (6) (1997) 1140–1147. doi:10.1107/S0021889897002173.
[64] G. D. Wignall, F. S. Bates, Absolute calibration of small-angle neutron scattering data, J. Appl. Cryst. 20 (1) (1987) 28–40. doi:10.1107/S0021889887087181.
[65] Lord Rayleigh, The incidence of light upon a transparent sphere of dimensions comparable with the wave-length, Proc. R. Soc. London A 84 (567) (1910) 25–46. doi:10.1098/rspa.1910.0054.
[66] A. Guinier, G. Fournet, Small-Angle Scattering of X-Rays, John Wiley & Sons, New York, 1955.
[67] R. H. Ottewill, A. R. Rennie, A. Schofield, The effect of electric fields on nonaqueous dispersions, in: M. Zulauf, P. Lindner, P. Terech (Eds.), Trends in Colloid and Interface Science IV, Vol. 81 of Prog. Colloid Polym. Sci., Steinkopff, 1990, pp. 1–5. doi:10.1007/BFb0115513.
[68] S. Ashdown, I. Marković, R. H. Ottewill, P. Lindner, R. C. Oberthür, A. R. Rennie, Small-angle neutron-scattering studies on ordered polymer colloid dispersions, Langmuir 6 (2) (1990) 303–307. doi:10.1021/la00092a002.
[69] P. Bartlett, R. H. Ottewill, Geometric interactions in binary colloidal dispersions, Langmuir 8 (8) (1992) 1919–1925. doi:10.1021/la00044a007.
[70] P. Bartlett, R. H. Ottewill, A neutron scattering study of the structure of a bimodal colloidal crystal, J. Chem. Phys. 96 (4) (1992) 3306–3318. doi:10.1063/1.461926.
[71] N. Mischenko, G. Ourieva, K. Mortensen, H. Reynaers, J. Mewis, SANS observations on weakly flocculated dispersions, Phys. B: Condens. Matter 234–236 (1997) 1024–1026. doi:10.1016/S0921-4526(96)01250-1.
[72] J. Stellbrink, J. Allgaier, D. Richter, A. Moussaid, A. B. Schofield, W. C. K. Poon, P. Pusey, P. Lindner, J. Dzubiella, C. Likos, H. Löwen, Partial structure factors in star polymer/colloid mixtures, Appl. Phys. A 74 (1) (2002) S355–S357. doi:10.1007/s003390101101.
[73] R. Kemp, R. Sanchez, K. J. Mutch, P. Bartlett, Nanoparticle charge control in nonpolar liquids: Insights from small-angle neutron scattering and microelectrophoresis, Langmuir 26 (10) (2010) 6967–6976. doi:10.1021/la904207x.
[74] G. N. Smith, S. Alexander, P. Brown, D. A. J. Gillespie, I. Grillo, R. K. Heenan, C. James, R. Kemp, S. E. Rogers, J. Eastoe, Interaction between surfactants and colloidal latexes in nonpolar solvents studied using contrast-variation small-angle neutron scattering, Langmuir 30 (12) (2014) 3422–3431. doi:10.1021/la500331u.
[75] G. N. Smith, I. Grillo, S. E. Rogers, J. Eastoe, Surfactants with colloids: Adsorption or absorption?, J. Colloid Interface Sci. 449 (2015) 205–214. doi:10.1016/j.jcis.2014.12.048.
[76] G. N. Smith, R. Kemp, J. C. Pegg, S. E. Rogers, J. Eastoe, Sulfosuccinate and sulfocarballylate surfactants as charge control additives in nonpolar solvents, Langmuir 31 (51) (2015) 13690–13699. doi:10.1021/acs.langmuir.5b03876.
[77] E. Di Cola, A. Moussaïd, M. Sztucki, T. Narayanan, E. Zaccarelli, Correlation between structure and rheology of a model

colloidal glass, J. Chem. Phys. 131 (14) (2009) 144903. doi:10.1063/1.3240345.
[78] S. M. Liddle, T. Narayanan, W. C. K. Poon, Polydispersity effects in colloid–polymer mixtures, J. Phys.: Condens. Matter 23 (19) (2011) 194116. doi:10.1088/0953-8984/23/19/194116.
[79] A. L. Washington, X. Li, A. B. Schofield, K. Hong, M. R. Fitzsimmons, R. Dalgliesh, R. Pynn, Inter-particle correlations in a hard-sphere colloidal suspension with polymer additives investigated by Spin Echo Small Angle Neutron Scattering (SESANS), Soft Matter 10 (17) (2014) 3016–3026. doi:10.1039/C3SM53027B.
[80] I. Grillo, Small-angle neutron scattering and applications in soft condensed matter, in: R. Borsali, R. Pecora (Eds.), Soft Matter Characterization, Springer Netherlands, 2008, pp. 723–782. doi:10.1007/978-1-4020-4465-6_13.
[81] A. Guinier, La diffraction dex rayons X aux très petits angles: Application à l'étude de phénomènes ultramicroscopiques, Ann. Phys. 12 (1939) 161–237.
[82] I. Marković, R. H. Ottewill, D. J. Cebula, I. Field, J. F. Marsh, Small angle neutron scattering studies on non-aqueous dispersions of calcium carbonate. Part I. The Guinier approach, Colloid Polym. Sci. 262 (8) (1984) 648–656. doi:10.1007/BF01452457.
[83] J. A. H. M. Moonen, C. G. Kruif, A. Vrij, S. Bantle, Small-angle neutron scattering of colloidal silica dispersions in a non-polar solvent, Colloid Polym. Sci. 266 (9) (1988) 836–848. doi:10.1007/BF01417868.
[84] W. G. Gall, N. G. McCrum, Internal friction in stereoregular polymethyl methacrylate, J. Polym. Sci. 50 (154) (1961) 489–495. doi:10.1002/pol.1961.1205015417.
[85] I. Marković, R. H. Ottewill, Small angle neutron scattering studies on nonaqueous dispersions of calcium carbonate Part 2. Determination of the form factor for concentric spheres, Colloid Polym. Sci. 264 (1) (1986) 65–76. doi:10.1007/BF01410309.
[86] J. K. Percus, G. J. Yevick, Analysis of classical statistical mechanics by means of collective coordinates, Phys. Rev. 110 (1) (1958) 1–13. doi:10.1103/PhysRev.110.1.
[87] W. C. K. Poon, E. R. Weeks, C. P. Royall, On measuring colloidal volume fractions, Soft Matter 8 (1) (2012) 21–30. doi:10.1039/C1SM06083J.
[88] S. R. Liber, S. Borohovich, A. V. Butenko, A. B. Schofield, E. Sloutskin, Dense colloidal fluids form denser amorphous sediments, Proc. Natl. Acad. Sci. U.S.A. 110 (15) (2013) 5769–5773. doi:10.1073/pnas.1214945110.
[89] L. D. Farrand, J. H. Wilson, S. Biggs, O. Cayre, S. Lawson, A. Richez, S. Stuart-Cole, Particles for electrophoretic displays, Patent WO 2013/170938 A1 (November 2013).
[90] B. Hammouda, Probing nanoscale structures—The SANS toolbox.
URL `http://www.ncnr.nist.gov/staff/hammouda/the_SANS_toolbox.pdf`
[91] M. J. Hollamby, Practical applications of small-angle neutron scattering, Phys. Chem. Chem. Phys. 15 (26) (2013) 10566–10579. doi:10.1039/C3CP50293G.
[92] K. L. Planken, H. Cölfen, Analytical ultracentrifugation of colloids, Nanoscale 2 (10) (2010) 1849–1869. doi:10.1039/C0NR00215A.
[93] T. M. Laue, W. F. Stafford III, Modern applications of analytical ultracentrifugation, Annu. Rev. Biophys. Biomol. Struct. 28 (1) (1999) 75–100. doi:10.1146/annurev.biophys.28.1.75.
[94] J. Lebowitz, M. S. Lewis, P. Schuck, Modern analytical ultracentrifugation in protein science: A tutorial review, Protein Sci. 11 (9) (2002) 2067–2079. doi:10.1110/ps.0207702.
[95] D. J. Growney, P. W. Fowler, O. O. Mykhaylyk, L. A. Fielding, M. J. Derry, N. Aragrag, G. D. Lamb, S. P. Armes, Determination of effective particle density for sterically stabilized carbon black particles: Effect of diblock copolymer stabilizer composition, Langmuir 31 (32) (2015) 8764–8773. doi:10.1021/acs.langmuir.5b01651.
[96] D. J. Growney, O. O. Mykhaylyk, L. Middlemiss, L. A. Fielding, M. J. Derry, N. Aragrag, G. D. Lamb, S. P. Armes, Is carbon black a suitable model colloidal substrate for diesel soot?, Langmuir 31 (38) (2015) 10358–10369. doi:10.1021/acs.langmuir.5b02017.
[97] D. J. Growney, O. O. Mykhaylyk, T. Derouineau, L. A. Fielding, A. J. Smith, N. Aragrag, G. D. Lamb, S. P. Armes, Star diblock copolymer concentration dictates the degree of dispersion of carbon black particles in nonpolar media: Bridging flocculation versus steric stabilization, Macromolecules 48 (11) (2015) 3691–3704. doi:10.1021/acs.macromol.5b00517.
[98] H. Müller, F. Herrmann, Simultaneous determination of particle and density distributions of dispersions by analytical ultracentrifugation, in: J. Behlke (Ed.), Analytical Ultracentrifugation, Vol. 99 of Prog. Colloid Polym. Sci., Steinkopff, 1995, pp. 114–119. doi:10.1007/BFb0114079.
[99] W. Wohlleben, M. Lechner, AUC and HDC characterization of heterogeneous polymer dispersions, Colloid Polym. Sci. 286 (2) (2008) 149–157. doi:10.1007/s00396-007-1771-0.
[100] Sigma–Aldrich.
URL `http://www.sigmaaldrich.com/united-kingdom.html`
[101] CRC, Viscosity of liquids, in: CRC Handbook of Chemistry and Physics, 95th Edition, CRC Press, 2014–2015 (Internet Version).
[102] D. S. Viswanath, T. Ghosh, D. H. L. Prasad, N. V. K. Dutt, K. Y. Rani, Viscosity of Liquids: Theory, Estimation, Experiment, Springer, Dordrecht, The Netherlands, 2007.
[103] O. Pekcan, M. A. Winnik, M. D. Croucher, A microphase model for sterically stabilized polymer colloids: Fluorescence energy transfer from naphthalene-labeled dispersions, J. Polym. Sci.: Polym. Lett. Ed. 21 (12) (1983) 1011–1018. doi:10.1002/pol.1983.130211208.
[104] O. Pekcan, M. A. Winnik, L. Egan, M. D. Croucher, Luminescence techniques in polymer colloids. 1. Energy-transfer studies in nonaqueous dispersions, Macromolecules 16 (4) (1983) 699–702. doi:10.1021/ma00238a038.
[105] O. Pekcan, M. A. Winnik, M. D. Croucher, Phosphorescence from covalently labeled nonaqueous dispersions: Insights into the swelling of microdomains: 2. Luminescence from polymer colloids, J. Colloid Interface Sci. 95 (2) (1983) 420–427.

doi:10.1016/0021-9797(83)90201-1.
[106] D. Vollmer, G. Hinze, B. Ullrich, W. C. K. Poon, M. E. Cates, A. B. Schofield, Formation of self-supporting reversible cellular networks in suspensions of colloids and liquid crystals, Langmuir 21 (11) (2005) 4921–4930. doi:10.1021/la047090w.